Revista Mexicana de Astronomía y Astrofísica Revista mexicana de astronomía y astrofísica ISSN: 0185-1101

Instituto de Astronomía, UNAM

Kimeswenger, S.; Barria, D.; Kausch, W.; Goldman, D. S. Emission line galaxies behind the planetary nebula IC 5148: Potential for a serendipity survey with archival data Revista mexicana de astronomía y astrofísica, vol. 54, no. 1, 2018, pp. 01-09 Instituto de Astronomía, UNAM

DOI: https://doi.org/10.14482/INDES.30.1.303.661

Available in: https://www.redalyc.org/articulo.oa?id=57171626007



Complete issue

More information about this article

Journal's webpage in redalyc.org

Scientific Information System Redalyc

Network of Scientific Journals from Latin America and the Caribbean, Spain and Portugal



EMISSION LINE GALAXIES BEHIND THE PLANETARY NEBULA IC 5148: POTENTIAL FOR A SERENDIPITY SURVEY WITH ARCHIVAL DATA

S. Kimeswenger^{1,2}, D. Barria¹, W. Kausch², and D. S. Goldman³

Received June 5 2017; accepted October 5 2017

ABSTRACT

During the start of a survey program using FORS2 long slit spectroscopy on planetary nebulae (PN) and their haloes, we serendipitously discovered six background emission line galaxies (ELG) with redshifts of $z=0.2057,\,0.3137,\,0.37281,\,0.4939,\,0.7424$ and 0.8668. Thus they clearly do not belong to a common cluster structure. We derived the major physical properties of the targets. Since the used long slit covers a sky area of only 570 arcsec² (= 4.3×10^{-5} square degrees), we discuss further potential of serendipitous discoveries in archival data, beside the deep systematic work of the ongoing and upcoming big surveys. We conclude that archival data provide a decent potential for extending the overall data on ELGs without any selection bias.

RESUMEN

Durante el comienzo de un programa de inspección usando espectroscopía de rendija larga con FORS2 en PNe y sus halos, descubrimos por casualidad seis galaxias de fondo con líneas de emisión (ELGs) con valores de corrimiento al rojo de $z=0.2057,\ 0.3137,\ 0.37281,\ 0.4939,\ 0.7424$ y 0.8668, respectivamente. Claramente estas galaxias no pertenecen a un cúmulo en común. Hemos derivado las principales propiedades físicas de estos objetos. Considerando que se ha usado una rendija larga que cubre un área del cielo de tan sólo 570 arcsec² (= 4.3×10^{-5} grados cuadrados), discutimos el futuro potencial del uso de datos de archivo para el descubrimiento casual de estos objetos, mas allá de los extensos programas de inspección actualmente en desarrollo y los futuros. Hemos concluido que estos datos de archivo representan un verdadero potencial para aumentar los datos sobre ELGs, sin efectos de selección.

Key Words: galaxies: active — galaxies: distances and redshifts — methods: observational — surveys — techniques: spectroscopic

1. INTRODUCTION

Emission line galaxies (ELGs) are frequently found in the universe. They are important to study environments of star formation and the more active environments in active galactic nuclei. New massive multi object (MOS) spectrograph surveys on ELGs (e.g. eBOSS on SDSS-IV) observe dedicated fields like the polar caps (see e.g. Delubac et al. 2017, and references therein) and will soon cover a few hundred thousand targets. They use selections by photometric characteristics of ELGs to position the slits. Tests have shown that this will introduce only a marginal

selection bias due to the size of the samples. The pilot survey already covered 9000 spectra (Comparat et al. 2016). A very recent survey of the Multi Unit Spectroscopic Explorer (MUSE) consortium during guaranteed time (Herenz et al. 2017) aiming in detection of ELGs will cover completely the area with this new instrument. No photometric selection is required as no MOS slits have to be positioned. It finally will cover 120 arcmin² of the CANDELS/Deep area of the Chandra Deep Field South.

On the other hand, serendipitous surveys are normally only carried out during space missions and analysis of space mission data, e.g. *The Cambridge-Cambridge ROSAT Serendipity Survey* (Boyle et al. 1995), *The ISO Serendipity Survey* (Klaas et al.

¹Instituto de Astronomía, UCN, Antofagasta, Chile.

²Institut f. Astro- und Teilchenphys., Innsbruck, Austria.

³Astrodon Imaging, Roseville, USA.

1997), The ASCA Hard Serendipitous Survey (della Ceca et al. 2001), The XMM-Newton Serendipitous Survey (Watson et al. 2001), The Swift XRT serendipitous deep survey (Moretti et al. 2006) and The NuSTAR Serendipitous Survey (Lansbury et al. 2017). Future plans also include next generation space telescopes like the James Webb Space Telescope incorporating the Medium Resolution Spectrometer (Bonato et al. 2017). They show that in addition to dedicated surveys, existing archival data provide a huge amount of data for serendipitous detections. As the observations were taken for other different purposes originally, these data will be free of any selection bias. In this paper we report on the discovery of six ELGs in FORS2 long-slit spectra taken within the framework of a detailed investigation of a recently discovered thin halo around the planetary nebula (PN) IC 5148 and discuss the potential of further serendipitous discoveries by a survey of the whole archive of this instrument.

2. DATA

The spectra were taken with the FOcal Reducer and low dispersion Spectrograph 2 (FORS2) (Appenzeller et al. 1998) mounted on the Cassegrain focus of ESO VLT UT1 (Antu) in the nights October 5th, 2016 from 3:15 to 4:03 UT, October 6th, 2016 from 0.15 to $0.30\,\mathrm{UT}$ and October 10^th , 2016 from 1:17 to 1:45 UT in service mode. In total 7 spectra were obtained, 3 with a position angle on the sky of 30° and 4 with a position angle of 150° (from N over E), trough the center of the PN IC 5148. The slit position was selected to cover some features of the wide halo of the PN. We used the long-slit mode of FORS2 since this enabled us to cover the entire halo using the full slit length of 6.78 with the standard collimator (slit width = 0.7). All spectra were taken with 14 minutes exposure time. We used the GRISM 300V and the GG435 order separation filter, covering a wavelength range from 455 to 889 nm. The MIT/LL CCD mosaic and the standard focal reducer collimator result in a 0".2518 pixel⁻¹ spatial resolution. This setup leads to a final wavelength dispersion of $0.33 \,\mathrm{nm}\,\mathrm{pixel}^{-1}$. The night sky lines were measured with a resolution $R = \Delta \lambda / \lambda$ of 200 and R = 360 at the blue end and the red end of the spectrum, respectively. We derived a FWHM of the stellar sources along the slit of about 1".17 at the blue end and 0".95 at the red part of the spectrum. This corresponds well to the reported DIMM seeing of the ESO meteo monitor of 1".1 @500 nm. The data were reduced incorporating the standard calibration mode using the ESO FORS pipeline v5.3.11

(Freudling et al. 2013). The resulting flux calibration was compared with the expected continuum flux of the central star of the PN finding differences of less than 2.5%. We used the software package molecfit (Smette et al. 2015; Kausch et al. 2015) to create a model of the telluric absorption lines by applying it on the high S/N central star spectrum. As the PN and its extended halo covered the whole slit length we used the software skycorr (Noll et al. 2014) to correct for the sky emission lines. This approach enabled us to derive a post correction of the wavelength calibration, too. Finally we averaged the spectra for each sky direction to achieve the final spectra of the faint sources used for this study.

3. RESULTS AND DISCUSSION

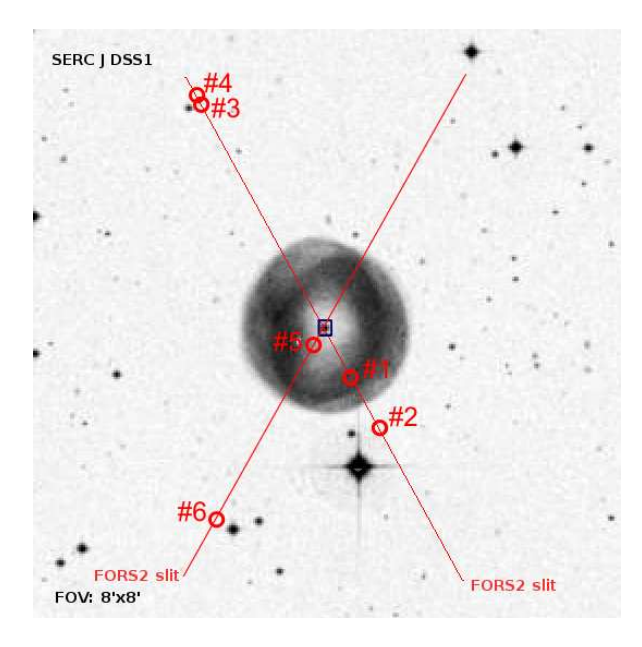
Figure 1 shows the field with the PN, and the slit including the positions of the ELGs. Since the targets are hardly visible on the Digitized Sky Survey (DSS) frame, we also show the 200 seconds HST WFPC2 exposure taken with the F814W filter, which covers the southern part of the PN and 3 of our targets.

Due to their different redshifts, clearly they do not belong to a common cluster structure. We derived the coordinates of target #1, #2 and #5 by means of the HST field; they are therefore more accurate than the coordinates of targets #3, #4 and #6, which were determined using the location of the emission lines in the slit relative to the central star of the PN.

To calculate the distances, luminosities and redshift based color corrections, we used the online cosmology calculator by Wright (2006), linked in the NASA/IPAC Extragalactic Database (NED). We further used the same cosmology ($H_0 = 73.0 \text{ km s}^{-1} \text{ Mpc}^{-1}$, $\Omega_{\text{Matter}} = 0.27$ and $\Omega_{\text{Vacuum}} = 0.73$) included in NED. The extinction correctection applied was the method of Schlegel et al. (1998) in the form recalibrated by Schlafly & Finkbeiner (2011).

3.1. Galaxy #1 (z = 0.2055): J215933.45-392343.9

This galaxy is completely covered by the main rim of the PN. The spectral regions around the emission lines are given in Figure 2. The nitrogen lines are only upper limits and the sulphur lines were marginally detected, since they are near the noise level. From the integrated spectrum of all 3 frames we obtained individual redshifts for the lines (c.f. Table 1).



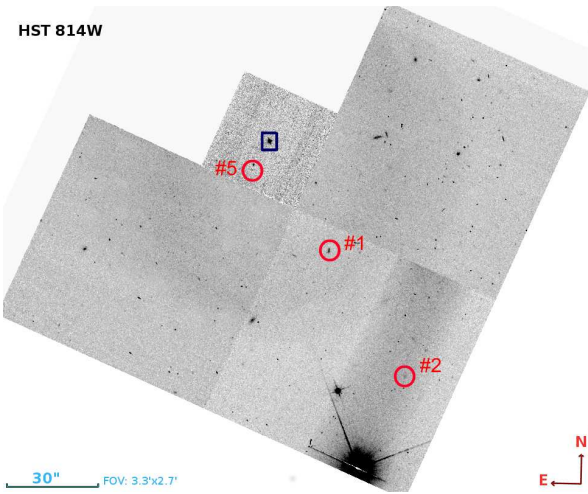


Fig. 1. Field around IC5148. The upper panel is based on the blue sky survey blue SERC DSS $J_{\rm ph}.$ The emission line galaxies are marked as circles. The lower panel covers the center of the field observed with the HST WFPC2 with a very red optical filter F814W. It shows three of the objects and a rich galaxy field behind the PN. The black square marks the central star of the PN. The color figure can be viewed online.

The H β line shows a slightly narrower profile and a slightly lower redshift than all the other lines. The profile was even somewhat narrower than that measured on the night sky lines. Since we removed a very strong He I line of the PN at its red edge we assume contamination and use only the blue part for a final fit of the intensity. Furthermore this line was not included to the total redshift calculation. The red-

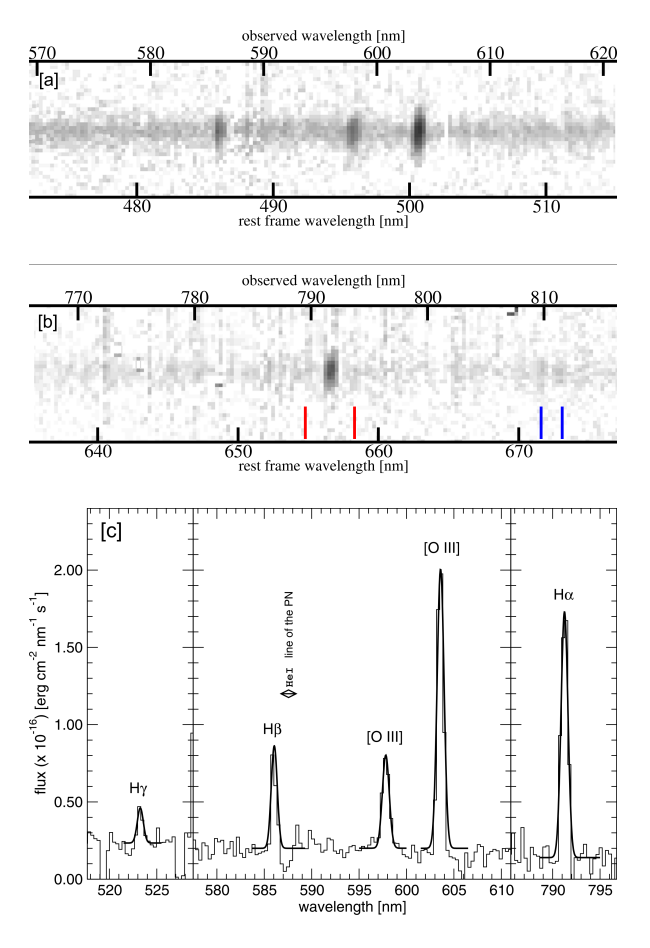


Fig. 2. Galaxy #1: The 2D spectrum around H β +[O III] (panel [a]) and around H α (panel [b]) and the integrated spectrum (panel [c]). The red ticks correspond to the redshifted wavelengths of the [N II] lines at 654.8 and 658.4 nm. The blue tics show the weak detection of the [S II] 671.6+673.1 nm pair. Each panel covers 50 nm in wavelength and 10" in spatial direction. We have chosen equal grey-scale for all those figures for easier comparison. The gray scale range is $[0.2 \times 10^{-19} \, \mathrm{erg \, cm^{-2} \, nm^{-2} \, s^{-1}}]$. Panel [c] shows the integrated spectrum of the galaxy and the best Gaussian fits as overlay. In the case of H β a strong contamination by the subtracted He I line of the PN exists (see text for more details). The color figure can be viewed online.

shifts, line intensities, target coordinates, the calculated distance modulus, and the line luminosities are summarized in Table 1. The Balmer series resembles a H $\alpha/{\rm H}~\beta$ line ratio which is nonphysical for electron temperatures above a few thousands of degrees (Osterbrock & Ferland 2006). Moreover, the H $\alpha/{\rm H}~\gamma$ is, within the expected errors of a few percent in line fluxes, as expected. We thus have to assume that

TABLE 1 SUMMARY OF THE OBSERVED PARAMETERS OF GALAXY #1

Position $\alpha_{\rm J2000} = 21^{\rm h}59^{\rm h}33.45$					
$\delta_{\rm J2000}=-39^{\rm o}23'43''.9$					
Ion	λ_{rest}	λ_{obs}	z	flux	
	nm	nm		[*]	
H γ	434.047	523.249	0.2055	2.0	
H β	486.135	585.968	$0.2054^{\rm a}$	6.1	
[O III]	495.891	597.800	0.2055	5.6	
	500.684	603.557	0.2055	16.7	
H α	656.279	791.254	0.2057	14.4	
[SII]	671.644	$809.694^{\rm b}$		≤ 0.7	
	673.082	$811.427^{\rm b}$		≤ 0.7	
Redshift $z_{\text{tot}} = 0.2055 \pm 0.0001$					
Luminosity $L_{\rm H\alpha} = 1.6 \times 10^{41} {\rm erg cm^{-2} s^{-1}}$					
$L_{\rm OIII} = 1.9 \times 10^{41} {\rm erg cm^{-2} s^{-1}}$					

^{*} Flux unit: $\times 10^{-16} \text{erg cm}^{-2} \text{ s}^{-1}$

the contamination of H β by the PN line mentioned above caused a flux error of up to 15% for this line. The continuum in the spectrum resembles that of a fairly blue object, although our blue cutoff at 450nm does not show the region around the Balmer jump at the given redshift.

3.2. Galaxy #2 (
$$z = 0.3720$$
):
 $J215931.28 - 392425.4$

This galaxy appears very faint on the HST/F814W image. There is a whole group of such low surface brightness objects on the image visible within a radius of about 0.5'. However, the emission lines are in good contrast to the sky background and the noise (see Figure 3, Table 2).

The galaxy is exceptionally bright in its O II emission (Table 2), although dust extinction would affect the oxygen line luminosity more than the hydrogen lines.

3.3. Galaxy #3 (z = 0.4937): J215944.0-392015

The coordinates of galaxy #3 in the slit correspond fairly well to those of the source USNO-B1 0506-0808786. Its $m_{\rm DSS,J}$ =21.^m1 also

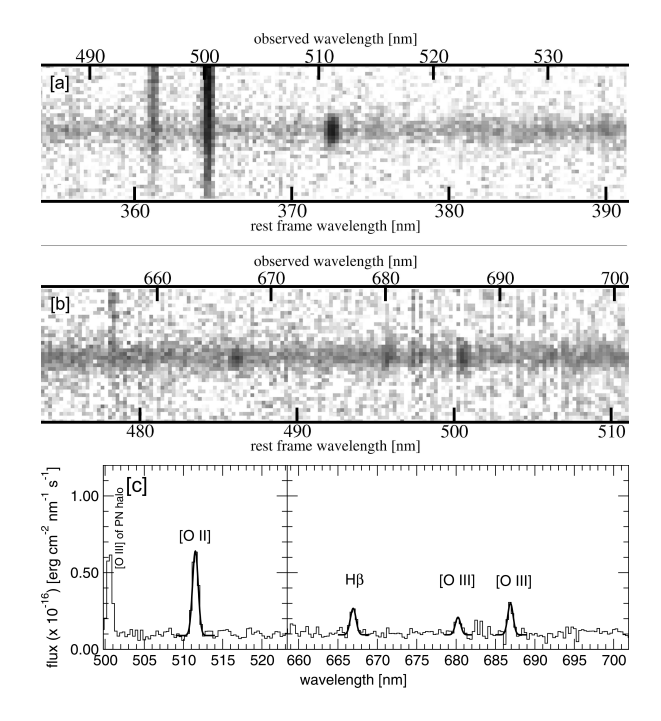


Fig. 3. Galaxy #2: The spectrum around [O II] (panel [a]) and H β +[O III] (panel [b]) using the same intensity scale and size as Figure 2. The lines crossing the whole upper panel are the O III halo emission lines of the PN. The integrated spectrum is given in panel [c] together with the best line fits in overlay.

TABLE 2 SUMMARY OF THE OBSERVED PARAMETERS OF GALAXY #2

Position	$\alpha_{\rm J2000} = 21^{\rm h}59^{\rm h}31.28$				
$\delta_{\rm J2000}=-39^{\rm o}24'24\rlap.{''}4$					
Ion	λ_{rest}	λ_{obs}	z	flux	
	nm	nm		[*]	
[O II]	372.742^{a}	511.512	0.3723	5.1	
H β	486.135	666.938	0.3719	1.6	
[O III]	495.891	680.236	0.3717	0.7	
	500.684	686.896	0.3719	1.9	
Redshift $z_{\rm tot} = 0.3720 \pm 0.0002$					
Luminosity $L_{\rm H\beta} = 7.1 \times 10^{40} \rm erg cm^{-2} s^{-1}$					
$L_{\rm OIII} = 8.4 \times 10^{40} {\rm erg cm^{-2} s^{-1}}$					
$L_{\rm OII} = 2.3 \times 10^{41} {\rm erg cm^{-2} s^{-1}}$					

^a Calculated as mean of 372.603 and 372.881 nm assuming about equal line strengths in the blend.

a Not included to calculate the value of z_{tot} due to PN contamination.

b Not measured, but calculated by z_{tot} .

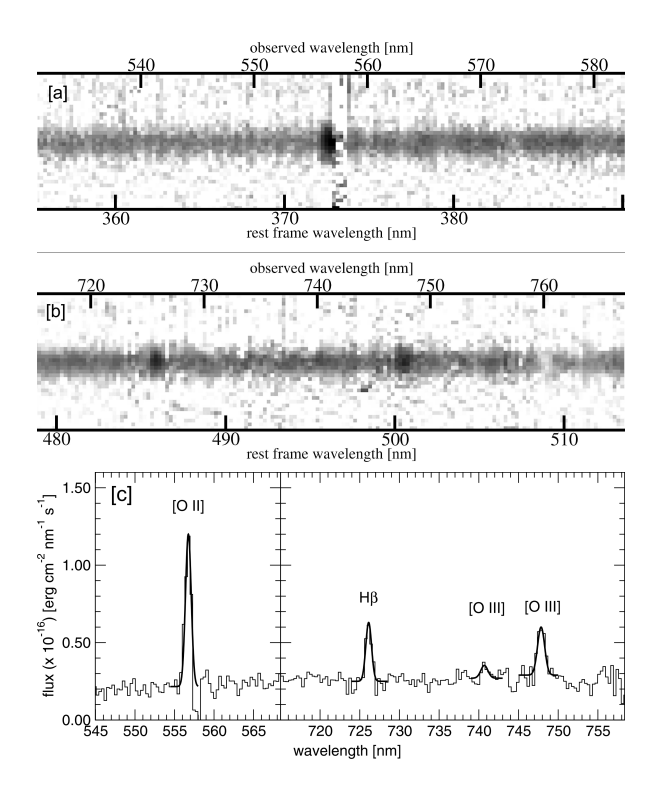


Fig. 4. Galaxy #3: The spectrum around [O II] (panel [a]) H β +[O III] (panel [b]) in the same intensity scale and size as Figure 2. The spectral range in the upper panel is contaminated by remnants of the sky substraction of the green O I airglow line at 557.7 nm. For the integrated spectrum (panel [c]) the blue O III line was fitted assuming a fixed line intensity ratio of 1:3 between the two oxygen lines. The color figure can be viewed online.

fits to the brightness of the continuum in the spectrum. The NED source GALEXASC J215944.22-392017.3 is 5'' westwards half way to the about 15magnitude 2MASS 21594450-3920191 source, which certainly was not in the slit of our spectrum. Although the coordinates of the GALEX source and the uncertainty of only 2"0 given in Seibert et al. (2012) do not fit well, we tend to believe that we identified this source, since it was detected only in the NUV band of the GALEX as a $5\,\sigma$ source (Figure 5). Despite its redshift of nearly 0.5, it is the brightest of the sources in the optical continuum (Figure 4). Values of log(O III/H β) = -0.09 and $\log(O II/H \beta) = +0.41$ (Table 3) also indicate that the galaxy is of composite type in the scheme of Marocco et al. (2011).

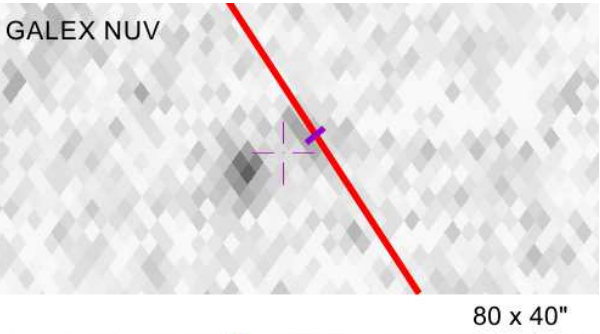
3.4. Galaxy #4 (z = 0.8668): J215943.7-392012

This target is only 3".2 northeast of galaxy #3. However, we found it to be the target with the highest redshift in our sample (Figure 6). Also, it is the

TABLE 3 SUMMARY OF THE OBSERVED PARAMETERS OF GALAXY #3

Position	$\alpha_{\rm J2000} = 21^{\rm h}59^{\rm h}44.0$			
	$\delta_{ m J2000}$	$=-39^{\circ}20$	′15″	
Ion	λ_{rest}	λ_{obs}	z	flux
	nm	nm		[*]
[O II]	$372.742^{\rm a}$	556.706	0.4935	9.0
H β	486.135	726.104	0.4936	3.5
[O III]	495.891	740.753	0.4938	$^{-b}$
	500.684	747.879	0.4937	2.9
Redshift $z_{\rm tot} = 0.4937 \pm 0.0001$				
Luminosity $L_{\rm H\beta} = 3.1 \times 10^{41} \rm erg cm^{-2} s^{-1}$				
$L_{\rm OIII} = 2.5 \times 10^{41} {\rm erg cm^{-2} s^{-1}}$				
$L_{\rm OII} = 8.0 \times 10^{41} {\rm erg cm^{-2} s^{-1}}$				

^a Calculated as mean of 372.603 and 372.881 nm assuming about equal line strengths in the blend.



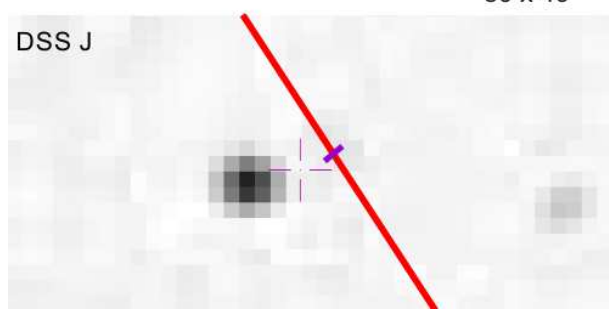


Fig. 5. Position of galaxy #3 (violet marker at the red FORS2 slit) on the blue DSS and the GALEX NUV band images. The cross marks the catalogue position of GALEXASC J215944.22-392017.3. The color figure can be viewed online.

b Only wavelength fitted - strength assumed 0.33 of the 500.684 nm line.

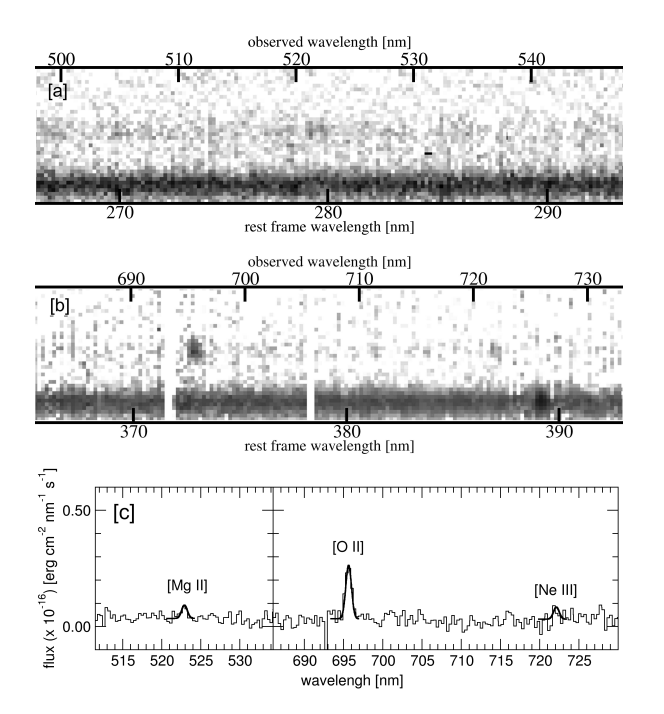


Fig. 6. Galaxy #4: The spectrum around [Mg II] (panel [a]) and around [O II] and [Ne III] (panel [b]). The bright target below is galaxy #3 with the H β at 726.10 nm. Panel [c] shows the integrated spectrum of the galaxy and the best Gaussian fits as overlay, as given before.

TABLE 4 SUMMARY OF THE OBSERVED PARAMETERS OF GALAXY #4

Position	$\alpha_{\rm J2000} = 21^{\rm h}59^{\rm h}43^{\rm s}.7$ $\delta_{\rm J2000} = -39^{\rm o}20'12''$			
Ion	λ_{rest}	λ_{obs}	z	flux
	nm	nm		[*]
[Mg II]	279.912	522.885	0.8677	0.5
[O II]	$372.742^{\rm a}$	695.621	0.8662	2.0
${ m NeIII}$	386.876	722.077	0.8664	0.5
Redshift $z_{\rm tot} = 0.8668 \pm 0.0008$				
Luminosity $L_{\rm OII} = 7.0 \times 10^{41} {\rm erg cm^{-2} s^{-1}}$				

^a Calculated as mean of 372.603 and 372.881 nm assuming about equal line strengths in the blend.

only target in our sample where the [Mg II] 279.8 nm UV line could be identified in the spectra (Table 4).

3.5. Galaxy #5 (z = 0.7424): J215935.61-2317.5

This target is very close to the PN center. Thus, the large variations of the PN emission lines do not

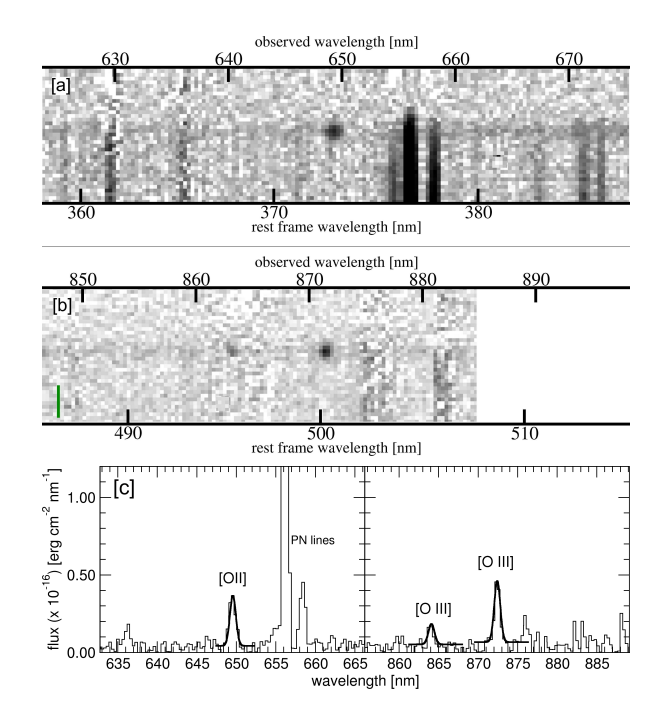


Fig. 7. Galaxy #5: Panel [a] shows strong remnants of the spatial inhomogeneous and thus only partially removed PN lines. The green mark in panel [b] shows the expected position of $H\beta$ which is lost due to bright OH telluric emission lines in that region. The right hand side is truncated due to the red end of our FORS2 setup. The integrated spectrum of the galaxy and the best Gaussian fits as overlay are shown in panel [c].

allow a complete removal of them (Figure 7). Although the redshift should allow the detection of the [Mg II] 279.8 nm UV line, we could not detect it, since its wavelength coincides exactly with that of the H β line of the PN. The H β line of the galaxy is lost in telluric emission lines of the OH molecule (Table 5).

3.6. Galaxy #6 (z = 0.3137): J215942.4-392530

This target is located behind the thin faint PN halo. Although the wavelength range covers the spectral region around H α , the [N II] and [S II] lines were not visible due to strong OH line contamination. (Figure 8, Table 5). The positional uncertainties of 0".6 given in the catalog of WISE J215942.81–392533.2 are inconsistent with the 3".5 distance to our target. Nevertheless, we believe these objects to be identical. Visual inspection of the WISE image (Cutri et al. 2013) at CDS/Aladin (Bonnarel et al. 2000) shows a very weak source at the detection limit and the bright stellar source

TABLE 5 SUMMARY OF THE OBSERVED PARAMETERS OF GALAXY #5

Position	$\alpha_{\rm J2000}$	$= 21^{h}59$	^h 35 ^s 61			
	$\delta_{\rm J2000} = -39^{\rm o}23'17''5$					
Ion	λ_{rest}	λ_{obs}	z	flux		
	nm	nm		[*]		
[O II]	372.742^{a}	649.484	0.7424	3.1		
[O III]	495.891	863.948	0.7422	1.1		
	500.684	872.414	0.7424	3.8		
Redshift $z_{\text{tot}} = 0.7424 \pm 0.0001$						
Luminosity $L_{\rm OII} = 7.4 \times 10^{41} {\rm erg cm^{-2} s^{-1}}$						
$L_{\rm OIII} = 9.0 \times 10^{41} {\rm erg cm^{-2} s^{-1}}$						

^a Calculated as mean of 372.603 and 372.881 nm assuming about equal line strengths in the blend.

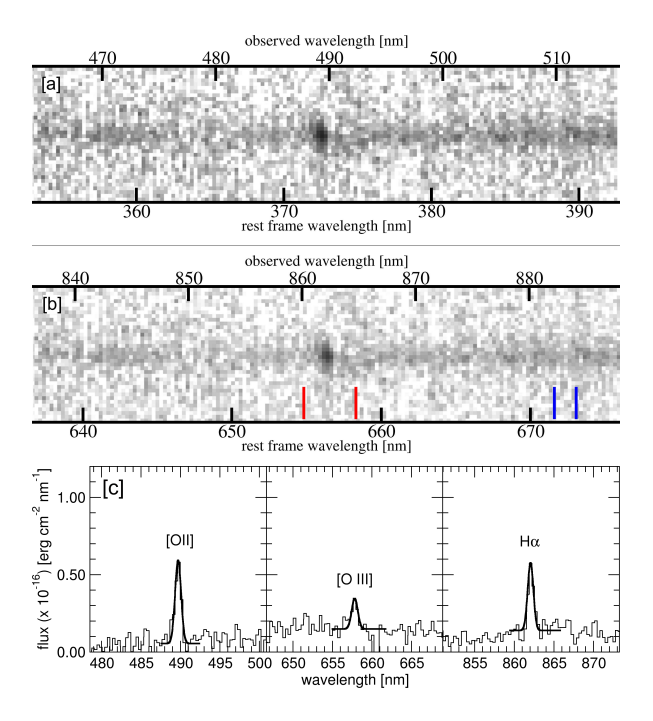


Fig. 8. Galaxy #6. Panel [a] shows the spectrum around $[O\,II]$. As in case of galaxy #1, the positions of the nitrogen and sulphur lines are given in panel [b]. However, due to strong telluric OH molecular lines in that region a detection was not possible. Panel [c] again shows the integrated spectrum.

WISE J215941.03-392547.1 nearby has a FWHM of 8".2 on the image (Figure 9). Thus the realistic positional error in the WISE data should be larger.

TABLE 6
SUMMARY OF THE OBSERVED PARAMETERS OF GALAXY #6

Position $\alpha_{\text{J}2000} = 21^{\text{h}}59^{\text{h}}42^{\text{s}}4$ $\delta_{\text{J}2000} = -39^{\text{o}}25'30''$					
Ion	λ_{rest}	λ_{obs}	z	flux	
	nm	nm		[*]	
[O II]	372.742^{a}	489.714	0.3138	4.6	
[O III]	495.891	651.602	$0.3140^{\rm b}$	0.6	
	500.684	657.786	0.3137	1.4	
Ηα	386.876	862.125	0.3137	4.0	

Redshift
$$z_{\rm tot} = 0.3137 \pm 0.0001$$

Luminosity $L_{\rm OII} = 4.6 \times 10^{41} {\rm erg \, cm^{-2} \, s^{-1}}$
 $L_{\rm OIII} = 4.3 \times 10^{40} {\rm erg \, cm^{-2} \, s^{-1}}$
 $L_{\rm H_{\alpha}} = 1.2 \times 10^{41} {\rm erg \, cm^{-2} \, s^{-1}}$

- ^a Calculated as mean of 372.603 and 372.881 nm assuming about equal line strengths in the blend.
- Not included to calculate value of $z_{\rm tot}$ due to line weakness.

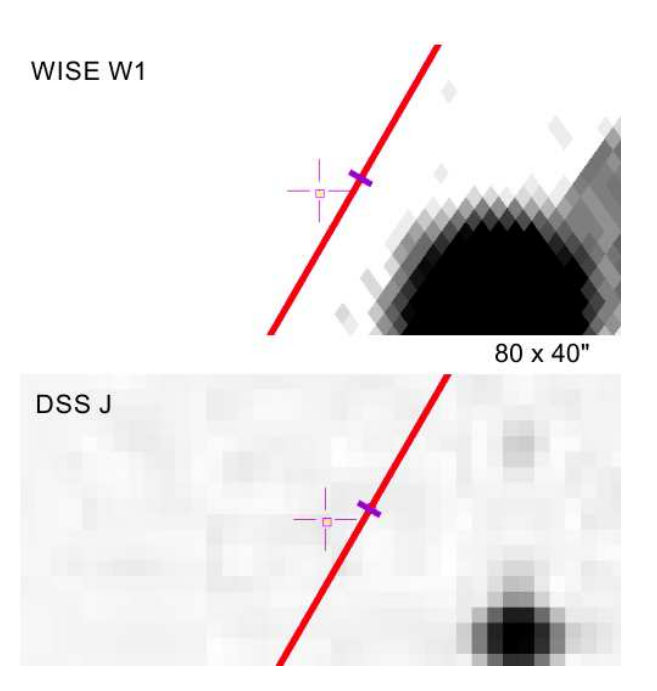


Fig. 9. Position of galaxy #6 (violet marker at the red FORS2 slit) on the blue DSS and the WISE W1 band images. The cross marks the catalogue position of WISE J214941.03-392547.1 .

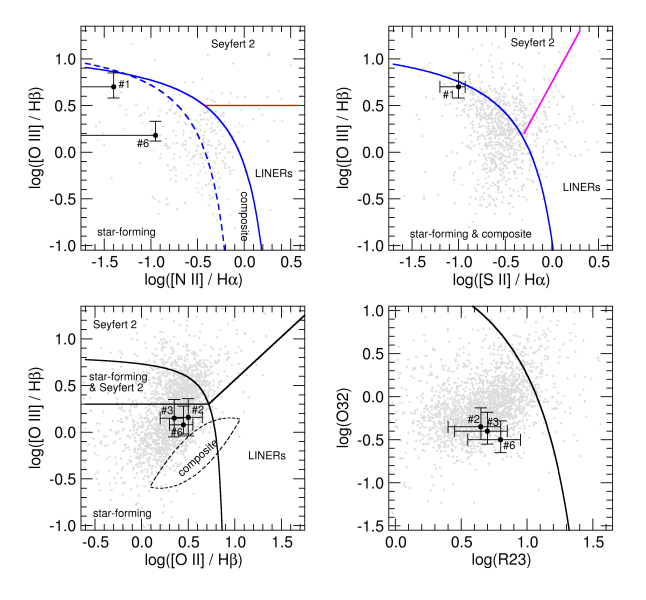


Fig. 10. Diagnostic diagrams following the classical BPT in the version of Lamareille (2010). The delimiter lines between the different galaxy types were defined by Veilleux & Osterbrock (1987), Kewley et al. (2001), Kauffmann et al. (2003) and Kewley et al. (2006). The underlying grey symbols are the galaxies of the VVDS. Open one-sided error bars denote upper limits.

4. DIAGNOSTIC DIAGRAMS

Although the sample is small and only a few line ratios are completely given one can obtain a first guess about these galaxies in the classical diagnostic diagrams following the BPT scheme (Baldwin et al. 1981). We applied the same analysis as proposed by Kewley et al. (2006), Lamareille (2010) and Marocco et al. (2011). As our sample covers a redshift domain from 0.2 < z < 0.9 we selected the VIMOS VLT Deep Survey (VVDS) data set of Lamareille et al. (2009), a large data set with the same redshift domain.

Galaxies #1 and #6 are the only ones with redshifts that allow us to investigate the region around H α . However, the [S II] and [N II] lines are limits or marginally detected, with large error bars. In the case of #6 the H β was estimated from the theoretical H $\alpha/{\rm H}\,\beta$ ratio and the calculation of the error bars assumes the unknown extinction to be $0 < A_{\rm V} < 3^{\rm m}$. For galaxies #2 and #3 we can use the blue line ratios directly (Figure 10). For #4 and #5 we do not have a complete pair of line ratios. All galaxies seem to belong to the family of normal star-forming galaxies, although #1 is very near to the border to the Seyfert 2 galaxies.

5. SUMMARY AND CONCLUSION

We reported on the discovery of six emission line galaxies within only two long-slit observation taken with the FORS2 spectrograph. The large spread of redshifts shows that these galaxies are not the result of a single bound cluster structure. Although upcoming large surveys on ELGs will give very good statistics in the near future, the serendipitous discoveries reported here show the potential of a survey based on the FORS2 ESO archive. Since we detected our sample in only two slit pointings covering a sky area of only 570 arcsec², we expect the number of further potential candidates to be very large, in particular since FORS2 has been in operation for more than a decade as one of the first-light VLT instruments. FORS2 is also one of the work horses at the VLT, and the spectrograph with the largest duty cycle without major changes among 8m class telescopes, leading to frequent scheduling and a high pointing coverage on the entire sky. Conducting a systematic serendipity survey based on FORS archival data will therefore lead to a large sample of ELGs completely unbiased by any selection criteria based on spatial distributions. That would be, to our knowledge, the very first attempt to use archival observations of optical slit spectroscopy to obtain a Serendipity Survey. Although the work of Thompson & Djorgovski (1995) is called Serendipitous Long-Slit Surveys for Primeval Galaxies, only its technique is comparable. It was obtained from dedicated pointing observations for this very extragalactic survey and not as a byproduct of other observations; thus, is restricted to a very limited deep field. Looking in the ESO archive we found about 20000 pointings at galactic latitudes above 20° and appropriate exposure times of >15 minutes. Moreover, using this approach we do not introduce a photometric pre-selection, as e.g. Delubac et al. (2017), allowing us to obtain an unbiased sample. The size of the telescope (much larger than the typical 2-4m class survey telescopes), and the exposures (often of one hour and more), will pick also galaxies with fairly small emission line contrast on top of their continuum.

As the publication of the first 20% of the MUSE-Wide survey (Herenz et al. 2017) shows, this instrument will add an additional possibility soon, when more data become public. They detected in the dedicated pointings 831 emission line galaxies in 22 arcmin² on the sky with 1 hour exposures. Their survey is 140 times larger and the exposure time was about a factor of 2 larger. Downsizing to our test area of 0.16 arcmin², the number of 5.9 expected detections is pretty much the same as we got. A future

extension to MUSE thus seems to be an attractive option too, although the required data handling will be more sophisticated.

The study is based on observations made with ESO Telescopes at the La Silla Paranal Observatory under programme ID 098.D-0332.

This research has made use of the SIMBAD database, operated at CDS, Strasbourg, France (Wenger et al. 2000), the NASA/IPAC Extragalactic Database (NED) which is operated by the Jet Propulsion Laboratory, California Institute of Technology, under contract with the National Aeronautics and Space Administration and has made use of "Aladin Sky Atlas" developed at CDS, Strasbourg Observatory, France (Bonnarel et al. 2000). Daniela Barria and this research were financed by the ALMA-CONICYT Fund, allocated to the project N° 31150001 and Wolfgang Kausch was supported by Project IS538003 (Hochschulraumstrukturmittel) provided by the Austrian Ministry for Research, Investigation and Economy (BM:wfw).

REFERENCES

- Appenzeller, I., Fricke, K., Fürtig, W., et al. 1998, Msngr, 94, 1
- Baldwin, J. A., Phillips, M. M., & Terlevich, R. 1981, PASP, 93, 5
- Bonato, M., Sajina, A., De Zotti, G., et al. 2017, ApJ, 836, 171
- Bonnarel, F., Fernique, P., Bienaymé, O., et al. 2000, A&AS, 143, 33
- Boyle, B. J., McMahon, R. G., Wilkes, B. J., & Elvis, M. 1995, MNRAS, 272, 462
- Comparat, J., Delubac, T., Jouvel, S., et al. 2016, A&A, 592, A121
- Cutri, R. M., Wright, E. L., Conrow, T., et al. 2013, Explanatory Supplement to the AllWISE Data Release Products, Tech. rep.
- della Ceca, R., Braito, V., Cagnoni, I., & Maccacaro, T. 2001, MmSAI, 72, 841

- Delubac, T., Raichoor, A., Comparat, J., & others. 2017, MNRAS, 465, 1831
- Freudling, W., Romaniello, M., Bramich, D. M., et al. 2013, A&A, 559, A96
- Herenz, E. C., Urrutia, T., Wisotzki, L., et al. 2017, A&A, 606, A12
- Kauffmann, G., Heckman, T. M., Tremonti, C., et al. 2003, MNRAS, 346, 1055
- Kausch, W., Noll, S., Smette, A., et al. 2015, A&A, 576, A78
- Kewley, L. J., Dopita, M. A., Sutherland, R. S., Heisler, C. A., & Trevena, J. 2001, ApJ, 556, 121
- Kewley, L. J., Groves, B., Kauffmann, G., & Heckman, T. 2006, MNRAS, 372, 961
- Klaas, U., Bogun, S., Herbstmeier, U., Lemke, D., et al. 1997, ASSL, 210, 45
- Lamareille, F. 2010, A&A, 509, A53
- Lamareille, F., Brinchmann, J., Contini, T., et al. 2009, A&A, 495, 53
- Lansbury, G. B., Stern, D., Aird, J., et al. 2017, ApJ, 836, 99
- Marocco, J., Hache, E., & Lamareille, F. 2011, A&A, 531, A71
- Moretti, A., Campana, S., Romano, P., et al. 2006, NCimb, 121, 1527
- Noll, S., Kausch, W., Kimeswenger, S., et al. 2014, A&A, 567, A25
- Osterbrock, D. E. & Ferland, G. J. 2006, Astrophysics of gaseous nebulae and active galactic nuclei, 2nd. ed. Sausalito, CA: University Science Books
- Schlafly, E. F. & Finkbeiner, D. P. 2011, ApJ, 737, 103 Schlegel, D. J., Finkbeiner, D. P., & Davis, M. 1998, ApJ, 500, 525
- Seibert, M., Wyder, T., Neill, J., et al. 2012, AAS 219, The Galaxy Evolution Explorer (GALEX) Source Catalogs, 340.01
- Smette, A., Sana, H., Noll, S., et al. 2015, A&A, 576, A77
- Thompson, D. & Djorgovski, S. G. 1995, AJ, 110, 982 Veilleux, S., & Osterbrock, D. E. 1987, ApJS, 63, 295
- Watson, M. G., Auguères, J.-L., Ballet, J., et al. 2001, A&A, 365, L51
- Wenger, M., Ochsenbein, F., Egret, D., et al. 2000, A&AS, 143, 9
- Wright, E. L. 2006, PASP, 118, 1711

- Stefan Kimeswenger and Daniela Barria: Instituto de Astronomía, Universidad Católica del Norte, Av. Angamos 0610, Antofagasta, Chile.
- Stefan Kimeswenger and Wolfgang Kausch: Institut für Astro- und Teilchenphysik, Leopold-Franzens Universität Innsbruck, Technikerstr. 25, 6020 Innsbruck, Austria.
- Don S. Goldman: Astrodon Imaging, 407 Tyrolean Court, Roseville, California, 95661, USA.